Spectroscopy investigation of nanostructured zinc ferrite obtained by mechanochemical synthesis

Z. Ž. LAZAREVIĆ[a,*], Č. JOVALEKIĆ[b], A. MILUTINOVIĆ[a], D. SEKULIĆ[c], M. ROMČEVIĆ[a], M. SLANKAMENAC[c], N. ROMČEVIĆ[a]
[a]*Institute of Physics, University of Belgrade, P.O. Box 68, Belgrade, Serbia*
[b]*The Institute for Multidisciplinary Research, University of Belgrade, Serbia*
[c]*Faculty of Technical Sciences, University of Novi Sad, Novi Sad, Serbia*

$ZnFe_2O_4$ has been obtained by soft mechanochemical synthesis in a planetary ball mill. $Zn(OH)_2$ and α-Fe_2O_3 are used as initial compounds. This mixture was activated mechanically for 18 h, uniaxially pressed and sintered at 1100°C/2h. The phase composition and cation distribution of the as-prepared and the sintered samples were analysed by XRD, Raman and IR spectroscopy and magnetic measurements. Morphology was examined by SEM. For investigation of the relaxation mechanism in the sintered $ZnFe_2O_4$ we used the complex impedance measurement, which suggested that the resistance of grain boundary and the resistance of bulk (grain) coexist in the temperature range 298-423 K and give adequate frequency-dependent responses.

(Received March 5, 2013; accepted September 18, 2013)

Keywords: $ZnFe_2O_4$, Raman spectroscopy, Magnetic properties

1. Introduction

The spinel ferrites are very important materials because of their excellent magnetic and electrical properties [1]. These materials have been used in many applications including electronics, magnetic storage, ferrofluid technology, as carriers for magnetically guided drug delivery, and as contrast agents in magnetically resonance imaging [2]. The chemical formula of the spinel ferrite can be written as MFe_2O_4, where *M* (*M* = Mn, Ni, Zn) is a divalent metal cation. The M^{2+} and Fe^{3+} cations can be distributed into two crystal sites of spinel structure: tetrahedral (A) and octahedral [B] sites. A whole range of distribution of cations is possible in ferrites, whose crystal chemical formula can be generally represented by $(M^{2+}_{1-\lambda}Fe^{3+}_{\lambda})[M^{2+}_{\lambda}Fe^{3+}_{2-\lambda}]O_4^{2+}$, where parentheses and square brackets denote cation sites of tetrahedral and octahedral coordination, respectively [3]. λ represents the so-called degree of inversion defined as the fraction of the (A) sites occupied by Fe^{3+} cations. The cation arrangement can vary between two extreme cases. One is the normal spinel ($\lambda = 0$), where all the divalent *M* cations occupy (A) sites and all the trivalent Fe cations occupy [B] sites. The other one is the inverse spinel ($\lambda = 1$), where all the divalent ions occupy [B] sites and trivalent cations are equally distributed between (A) and [B] sites. Spinels with the cation distribution intermediate between normal and inverse (i.e., partially inverse spinels; $0 < \lambda < 1$) are also very frequent.

Many methods, such as traditional ceramic synthesis [4], hydrothermal synthesis [5], sol-gel techniques [6], co-precipitation [7], mechanical milling [8, 9] etc., have been used to fabricate the ferrites starting from various precursors. Mechanochemical processing is a novel and low- cost effective method of producing a wide range of nanopowders. It involves the use of a high energy ball mill to initiate chemical reactions and structural changes. It was shown that mechanochemical processing is a very promising technique that can be applied to the synthesis and processing of various high-tech materials. Soft mechanochemical synthesis method developed by Senna [10] posseses some advantageous because highly reactive compounds containing oxygen-hydrogen groups are used as a precursors. In fabricating of ferrites used method and sintering temperature dramatically affect the crystal sizes and cation distribution.

Zinc ferrite is not only interesting in basic researches in magnetism, but also has great potential in technological application. Previously, we have prepared $MnFe_2O_4$ and $NiFe_2O_4$ ferrites [11, 12]. The objective of present work is primarily to prepare of $ZnFe_2O_4$ ferrite by soft mechanochemical synthesis and to study this ferrite using different methods of characterization.

2. Experimental procedures

For The following crystalline powders were used as starting materials: zinc(II)-hydroxide ($Zn(OH)_2$, Merck 95% purity) and hematite (α-Fe_2O_3, Merck 99% purity). Soft mechanochemical synthesis was performed in air atmosphere in planetary ball mill (Fritsch Pulverisette 5) for 18 h. The powder mixture was pressed into pallet using a cold isostatic press (8 mm in diameter and ~3 mm thick and sintered at 1100 °C for 2 h (Lenton-UK oven) without pre-calcinations step. Heating rate was 10 °C min^{-1}, with

nature cooling in air atmosphere. Characterization of the obtained samples was carried out by several methods.

The formation of phase and crystal structure of the $ZnFe_2O_4$ was verified via the X-ray diffraction measurements (XRD). Model Philips PW 1050 diffractometer equipped with a PW 1730 generator (40 kV x 20 mA) was used with Ni filtered CoKα radiation of 1.78897 Å at the room temperature. Measurements were done in 2θ range of 15-80° with scanning step width of 0.05° and 10 s scanning time per step.

Raman measurements of mixture powder and sintered sample were performed using Jobin-Ivon T64000 monochromator. An optical microscope with 100x objective was used to focus the 514 nm radiation from a Coherent Innova 99 Ar^+ laser on the sample. The same microscope was used to collect the backscattered radiation. The scattering light dispersed was detected by a charge-coupled device (CCD) detection system. Room temperature Raman spectra are in spectral range from 100 to 800 cm^{-1}.

The infrared (IR) measurements were carried out with a BOMMEM DA-8 FIR spectrometer. A DTGS pyroelectric detector was used to cover the wave number range from 50-700 cm^{-1}.

The microstructure of sintered sample was examined using scanning electron microscope (SEM, Model Sirion 200 SITP, operated at 10 kV).

The magnetization measurements were done at room temperature using VSM 200 cryogenic magnetometer in magnetic field from 0 kOe to ± 80 kOe.

Impedance measurements were carried out in the frequency range 100 Hz to 10 MHz on a HP-4194A impedance/gain-phase analyzer using a HP-16048C test fixture at the temperature of 298-423 K.

2. Results and discussion

Fig. 1 show the X-ray diffraction patterns of $ZnFe_2O_4$ powder obtained from stoichiometric mixture of powders $Zn(OH)_2$ and α-Fe_2O_3 in a ball mill for 18 h and after sintered at 1100 °C for 2 h. Both, the powder and sintered $ZnFe_2O_4$ are single-phase ferrites with spinel structure. To get more information, the crystallite sizes of powder and sintered sample were calculated from X-ray peak broadening using the Scherrer formula [13]:

$$L = K\,\lambda_{Co} / (\beta \cos \theta_{hkl}) \qquad (1)$$

where L is the crystallite size, λ_{Co} is the wavelength of X-ray radiation (1.78897 Å for Co-K_α), θ_{hkl} is the Bragg angle and β is the full width at half maximum (FWHM) of the diffraction peak (reflection from (*hkl*) crystal plane) reduced for instrumental broadening. K is a Scherrer constant. The estimated average particle size is 13 nm for powder and 100 nm for the sample sintered at the temperature of 1100 °C for 2 h.

The obtained XRD patterns show clear peaks whose positions and relative intensities correspond to the bulk $ZnFe_2O_4$ (JCPDS card 89-7412) and are well indexed as cubic spinel phase with the *fcc* structure [14]. The diffractograms show different reflection planes indexed as (*hkl*): (111), (220), (311), (222), (400), (422), (511) and (440). Based on the measured positions of diffraction peaks it can be calculated lattice constant by well-known relation:

$$a = \lambda_{Co}\,(h^2 + k^2 + l^2)^{1/2}/(2\sin\theta_{hkl}) \qquad (2)$$

Calculated lattice constant for sintered sample is a = 0.8419 nm, slightly (0.035%) less than in the bulk (JCPDS card 89-7412, a = 0.8422 nm). Lattice constant of powder sample is 0.8402 nm, 0.24% less than crystal lattice constant, what indicates presence of nano effects.

Raman spectra of samples obtained from mixture of $Zn(OH)_2$ and α-Fe_2O_3 powders for 18 h milling time and after sintered are analyzed by deconvolution (Fig. 2). Crystal $ZnFe_2O_4$ has normal spinel structure. The group theory predicts 5 Raman active modes in spinel structure: $A_{1g} + E_g + 3F_{2g}$. All five Raman peaks in sintered $ZnFe_2O_4$ are clearly visible and have symmetric form, what is a characteristic of normal spinel structure. Raman spectra of $ZnFe_2O_4$ nanocrystalline samples, obtained by mechanochemical method at low temperature have visible doublets and it could be concluded that spinel structure of these samples is mostly inversed.

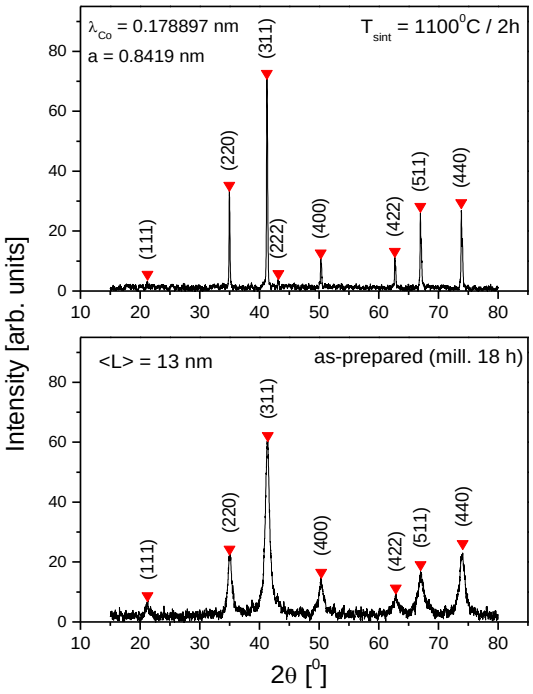

Fig. 1. X-ray diffraction patterns of the $ZnFe_2O_4$ obtained for 18 h milling time and after sintered at 1100 °C for 2 h.

In the cubic ferrites, the strongest modes above 600 cm^{-1} correspond to symmetric stretching of oxygen in tetrahedral AO_4 groups, so the modes about 630 cm^{-1} can be reasonably considered as A_g symmetry. E_g (~ 250 cm^{-1}) is due to symmetric bending of oxygen with respect to cation in tetrahedral surrounding. $F_{2g}(2)$ (~ 350 cm^{-1}) and

$F_{2g}(3)$ (~ 450 cm^{-1}) correspond to the vibrations of octahedral group: $F_{2g}(2)$ is due to asymmetric stretching and $F_{2g}(3)$ is caused by asymmetric bending of oxygen. $F_{2g}(1)$ (~ 160 cm^{-1}) is due to translational movement of the whole tetrahedron. Double modes in the as-prepared 18 h milled sample imply that ordered sublattice of Zn ions in tetrahedral sites exist together with sublattice of Fe-ions.

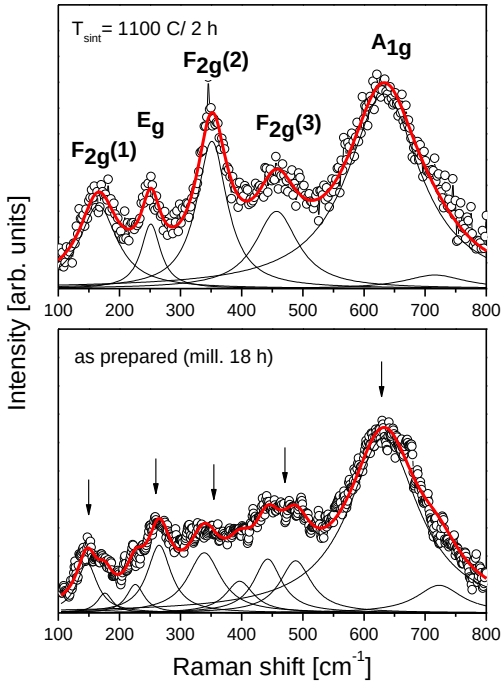

Fig. 2. Raman spectra at room temperature of the $ZnFe_2O_4$ obtained for 18 h milling time and after sintered at 1100 ℃ for 2 h.

For further characterization of the synthesized $ZnFe_2O_4$ ferrite, IR spectra were recorded in the range of 50-700 cm^{-1} (Fig. 3), where all the group theory predicted spinel modes (4 F_{1u}) are expected to be [15]. The most exaggerated features in spectra, $F_{1u}(3)$ and $F_{1u}(4)$, correspond to the stretching of cation-oxygen bond in in octahedral and tetrahedral sites, respectively. It is known that the higher band at ~700 cm^{-1} corresponds to the intrinsic vibrations of tetrahedral site and the lower band at ~400 cm^{-1} is attributed to the vibrations of octahedral site. The different values of the energy position for these modes are due to different values of metal ion - O^{2-} distances for octahedral and tetrahedral sites. In reflectivity spectra of $ZnFe_2O_4$ TO-LO splitting of the most intensive $F_{1u}(4)$ IR mode is visible. Fitted values of TO and LO modes in the sintered sample agree well with values in bulk. Values of the corresponding modes in the as-prepared powder sample are expectedly modified due to superposition of bulk and surface effects.

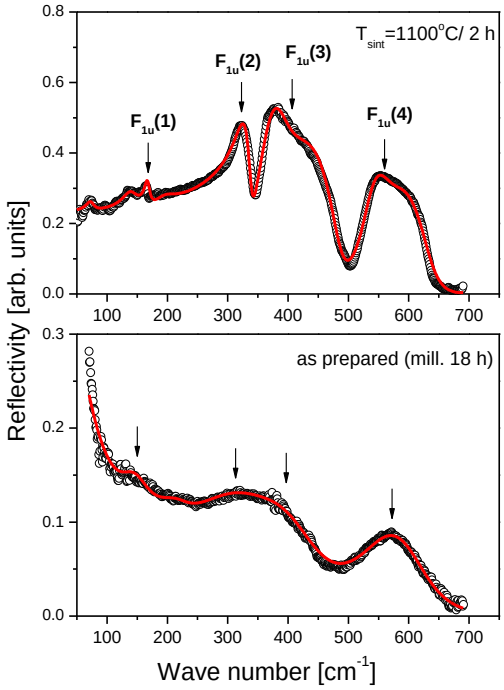

Fig. 3. IR spectra at room temperature of the $ZnFe_2O_4$ obtained for 18 h milling time and after sintered at 1100 ℃ for 2 h.

Fig. 4 shows the SEM micrograph for the sample obtained from the mixture of $Zn(OH)_2$ and α-Fe_2O_3 powders by the soft mechanochemical synthesis for 18 h milling time, than sintered at 1100 °C for 2 h. The sintered zinc ferrite consists of polygonal grains, with relatively homogeneous grain distribution, with an average grain size varying from 0.2-1 μm. It is well known that the microstructure of materials strong influences on the magnetic and electrical properties, so it will be done detailed research in the future.

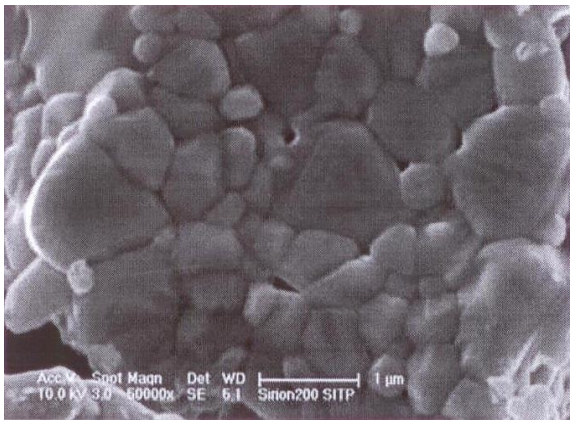

Fig. 4. SEM micrograph image of the $ZnFe_2O_4$ sintered at 1100 ℃ for 2h.

The magnetization curves of the zinc ferrite measured at room temperature are shown in Fig. 5. Sintered sample

exhibits a paramagnetic behavior, what is expected in the case of bulk, or crystalline material with crystalline size of 100 nm order. Such material is practically without internal tensions and in the case of sintered $ZnFe_2O_4$ a normal spinel structure with fully populated antiferromagnetic tetrahedral [B] sites is established. ([B] - [B] superexchange interaction is weak and bulk $ZnFe_2O_4$ became antiferromagnetic at about 10 K.) On the other hand, in the as-prepared sample with nano-sized crystallites can be recognized a superparamagnetic behavior [16, 17]. The estimated value of saturation magnetization is M_{sat} = 51.13 emu/g what is a result of the inversion of cations. The largest superexchange interaction in spinel ferrites, in the case of $ZnFe_2O_4$ established between Fe^{3+} ions in (A) and [B] sites, generates such high value of magnetisation. Nano-powder of $ZnFe_2O_4$ in the as-prepared sample is predominantly of mono-domen crystallites what is confirmed by a small remanence magnetization, M_{rem} = 5 emu/g. Open hysteresis loop, with coercive field, H_{coerc} = 100 Oe (in combination with high magnetization), shows that ferrimagnetic transition temperature is well above the room temperature. The fact that magnetization does not achieve a saturation in the magnetic fields up to ± 80 kOe implies a surface spin disorder. Ordering of these spins in a magnetic field contributes in the magnetic moment of the mono-domen $ZnFe_2O_4$ crystallites, also.

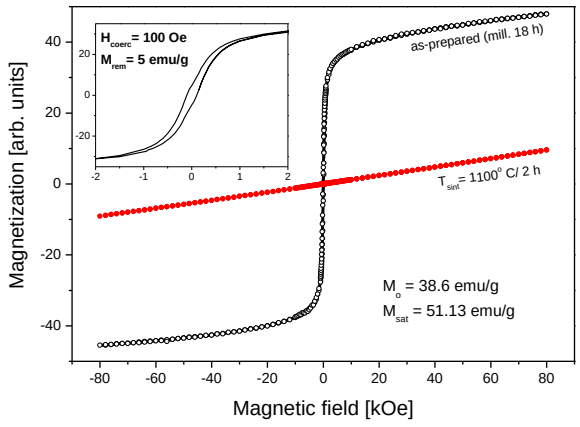

Fig. 5. Magnetic measurements of the $ZnFe_2O_4$ obtained for 18 h milling time and after sintered at 1100 ℃ for 2 h.

In the present investigation, the impedance spectroscopy [18] is used as well-developed tool to study the electrical properties of ferrites. By using this method, the AC response can be modeled with two semi-circles in the impedance plane; the first in a low frequency domain represents the impedance of grain boundary. The second one obtained in a high frequency domain corresponds to the impedance of grain or bulk properties [19]. *Cole-Cole* plots of impedance data for sintered $ZnFe_2O_4$ ferrite as a function of frequency at different temperatures are presented in Fig. 6. As one can see, the impedance spectrum shows presence of two semi-circles for measured frequency range 100 Hz -10 MHz. It suggests that there are two effects pertaining to the microstructural inhomogeneity: grain and grain boundary. The diameters of these semi-circles exhibit decreasing trends with the increase in temperature. This indicates that the conductivity increases with increase in temperature supporting the negative temperature coefficient of resistance behavior of the $ZnFe_2O_4$ usually shown by semiconductors. Additionally, the impedance value of investigated zinc ferrite decreases by two orders of magnitude, which is due to thermal activation mechanism [20]. The rise of temperature brings to an enhanced conductivity, and hence, decreasing the impedance values.

Successful modeling of the impedance response is achieved using an equivalent circuit consisting of two serially connected parallel *R-CPE* elements taking into account grain and grain boundary effects, see *inset* in Fig. 6. Here R_g and R_{gb} correspond to the grain and grain boundary resistance and CPE_g and CPE_{gb} are the constant phase elements for grain interiors and grain boundaries, respectively. The constant phase element (*CPE*) is used to accommodate the nonideal Debye-like behavior of the capacitance which is given by relation $C = Q^{1/n}R^{(1-n)/n}$, where the value of parameter n is 1 for a pure capacitor [21]. The electrical parameters of proposed circuit were calculated for every temperature measurement by analyzing the impedance data using EIS Spectrum Analyzer software [22] and are given in the Table 1. It is observed that resistance and capacitance have higher values for the grain boundary than for the grain. The fact that the capacitance of grain boundary (C_{gb}) is larger than capacitance of grain (C_g) can be explained on the basis that capacitance is inversely proportional to the thickness of the media. As temperature increases, both the grain resistance (R_g) and grain boundary resistance (R_{gb}) are found to decrease, which is indicated by a shift in the radius of the semicircular arcs towards left side of the real (Z') axis. This provides convincing evidence that the electrical properties of sintered $ZnFe_2O_4$ ferrite are dependent on microstructure as well as temperature. Since the relaxation time of grain ($\tau_g = R_gC_g$) and grain boundary ($\tau_{gb} = R_{gb}C_{gb}$) are different, the impedance spectroscopy allows separation of those. For temperature range from 298 K to 423 K, the calculated values of τ_g of the $ZnFe_2O_4$ sample fall in the range of 7.78 μs to 0.068 μs, respectively. Besides, the calculated values for τ_{gb} are from 8.31 ms to 0.312 ms in the same temperature range. In addition, grain boundary relaxation times are about three orders of magnitude larger than those of the grain-interior. This means that in the grain boundary structure the time spent in the relaxation process is longer. Also, it is observed that the decrease of both resistances with increasing temperature results in the decrease of relaxation time. This variation of relaxation times with temperature is a clear proof that the relaxation process is temperature dependent [23-25].

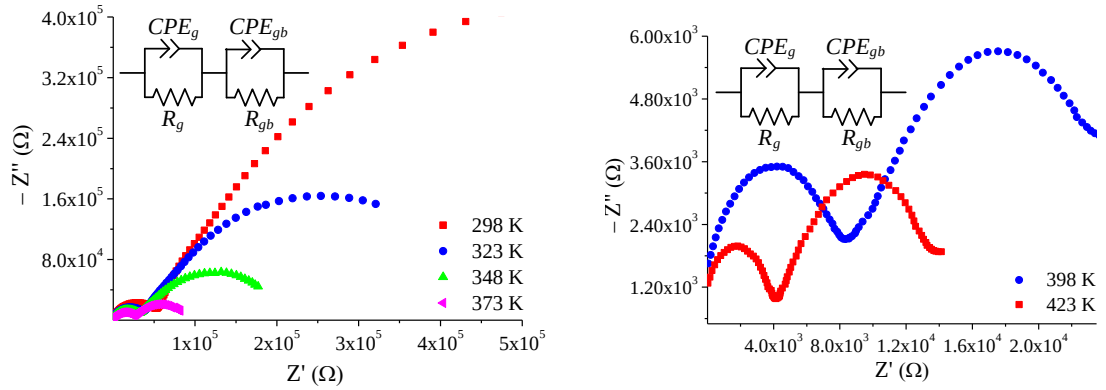

Fig. 6. Cole-Cole plots for the sample of the $ZnFe_2O_4$ ferrite at different temperatures. Inset: proposed equivalent circuit model for analysis of the impedance spectroscopy data.

Table 1. Impedance parameters calculated from the complex impedance plots at different temperatures.

T [K]	R_g [Ω]	C_g [F]	n_g	R_{gb} [Ω]	C_{gb} [F]	n_{gb}
298	5.44E+04	1.43E-10	0.83979	1.17E+06	7.11E-09	0.80709
323	3.98E+04	2.35E-10	0.82919	4.51E+05	9.53E-09	0.79713
348	3.42E+04	3.00E-10	0.81115	1.77E+05	1.36E-08	0.78479
373	2.45E+04	1.66E-10	0.85086	6.53E+04	2.87E-08	0.72616
398	7.80E+03	7.81E-11	0.89961	1.89E+04	4.58E-08	0.69429
423	3.87E+03	1.76E-11	0.98706	1.08E+04	2.89E-08	0.74088

4. Conclusions

In this paper, we obtained $ZnFe_2O_4$ ferrite by soft mechanochemical synthesis starting from the mixture of $Zn(OH)_2$ and α-Fe_2O_3 powders and sintered at 1100 °C/2h. It has been shown that mechanochemical treatment of mixture with starting materials leads to forming the phase of $ZnFe_2O_4$ after 18 h of milling. In the Raman and IR spectra are observed all of the group theory predicted first-order active modes characteristic for spinel structure. Raman modes of sintered $ZnFe_2O_4$ are in the form characteristic for normal spinel structure, and in the case of powder, Raman spectra show a presence of cation inversion. A high magnetization of a milled sample confirms cation inversion, also. Sintered sample has a normal spinel structure and, as a consequence, paramagnetic behavior at 300 K. The sintered $ZnFe_2O_4$ consists of the polygonal grains. The analysis of the complex impedance data shows that the capacitive and reactive properties of the sintered $ZnFe_2O_4$ ferrite are mainly attributed due to the processes which are associated with the grain and grain boundary. Also, it is seen that the radius of curvature of *Cole-Cole* plots is decreased with increasing temperature, suggesting a mechanism of temperature-dependent on relaxation.

Acknowledgements

This research was financially supported by the Ministry of Education, Science and Tehnological Development of the Republic of Serbia through Projects No. III45003 and III43008.

References

[1] M. J. Nasr Isfahani, M. Myndyk, V. Šepelák, J. Amighian, J. Alloy Compd. **470**, 434 (2009).
[2] V. Šepelák, P. Heitjans, K. D. Becker, J. Therm. Anal. Calorim. **90**, 93 (2007).
[3] S. H. Pradhan, S. Bid, M. Gateshki, V. Petkov, Mater. Chem. Phys. **93**, 224 (2005).
[4] C. N. Chinnasamy, A. Narayanasamy, N. Ponpandian, K. Chattopadhyay, H Guérault, J-M. Greneche, J. Phys.- Condens. Mat. **12**, 7795 (2000).

[5] S. H. Yu, T. Fujino, M. Yoshimura, J. Magn. Magn. Mater. **256**, 420 (2003).
[6] S. Khorrami, F. Gharib, G. Mahmoudzadeh, S. Sadat Sepehr, S. Sadat Madani, N. Naderfar, S. Manie, Int. J. Nano. Dim. **1**, 221 (2011).
[7] M. Maletin, Ž. Cvejić, S. Rakić, L. M. Nikolić, V. V. Srdić, Mater. Sci. Forum **518**, 91 (2006).
[8] S. Mornet, S. Vasseur, F. Grasset, P. Veverka, G. Goglio, A. Demourgues, J. Portier, E. Pollert, E. Dugust, Prog. Solid State Chem. **34**, 237 (2006).
[9] T. F. Marinca, I. Chicinaş, O. Isnard, V. Pop, Optoelectron. Adv. Mater. – Rapid Comm. **5**, 39 (2011).
[10] M. Senna, in Powder Technology Handbook, 3rd Edition, Eds. H. Masuda, K. Higashitani, H. Yoshida, CRC Press, Boca Raton, 2006.
[11] Z. Ž. Lazarević, Č. Jovalekić, A. Rečnik, V. N. Ivanovski, M. Mitrić, M. J. Romčević, N. Paunović, B. Đ. Cekić, N. Ž. Romčević, J. Alloys Compd. **509**, 9977 (2011).
[12] Z. Ž. Lazarević, Č. Jovalekić, A. Milutinović, M. J. Romčević, N. Ž. Romčević, Acta. Phys. Pol. A **121**, 682 (2012).
[13] Scherrer and Warren equations (B. E. Warren, X-ray Diffraction, Addison Wesley: Reading MA, (1969).
[14] Y. Li, R. Yi, A. Yan, L. Deng, K. Zhou, X. Liu, Solid State Sci. **11**, 1319 (2009).
[15] R. D. Waldron, Phys. Rev. **99**, 1727 (1955).
[16] C. N. Chinnasamy, A. Narayanasamy, N. Ponpandian1, K. Chattopadhyay, H. Guérault, J-M. Greneche, Scripta Mater. **44**, 1407 (2001).
[17] C. Yao, Q. Zeng, G. F. Goya, T. Torres, J. Liu, H. Wu, M. Ge, Y. Zeng, Y. Wang, J. Z. Jiang, J. Phys. Chem. C **111**, 12274 (2007).
[18] N. Bonanos, B. C. H. Steele, E. P. Butler, in Impedance Spectroscopy: Theory, Experiment, and Applications, 2nd Edition, Eds. E. Barsoukov, J. R. Macdonald, John Wiley&Sons, 2005, pp. 205-343.
[19] W. Chen, W. Zhu, O. K. Tan, X. F. Chen, J. App. Phys. **108**, 0341011 (2010).
[20] Z. Lazarević, A. Milutinović, M. Romčević, N. Romčević, Č. Jovalekić, D. Sekulić, M. Slankamenac, ISAF ECAPD PFM 2012, Aveiro, Portugal, the USBs electronic conference Proceedings, No 07 (2012).
[21] M. Younas, M. Nadeem, M. Atif, R. Grossinger, J. App. Phys. **109**, 093704 (2011).
[22] A. S. Bondarenko, G. A. Ragoisha, EIS Spectrum Analyser (a freeware program for analysis and simulation of impedance spectra), see http://www.abc.chemistry.bsu.by/vi/analyser/.
[23] S. Dutta, R. N. P. Choudhary, P. K. Sinha, Ceram. Int. **33,** 13 (2007).
[24] Z. Ž. Lazarević, Č. Jovalekić, D. L. Sekulić, M. P Slankamenac, M. Romčević, A. Milutinović, N. Ž. Romčević, Sci. Sinter. **44**, 331 (2012).
[25] K. Verma, S. Sharma, Phys. Status Solidi B **249**, 209 (2012).

*Corresponding author: lzorica@yahoo.com